Available online at www.sciencedirect.com
SCIENCE DIRECT®
Aerospace Science and Technology 8 (2004) 63–71
Aerospace Science and Technology
www.elsevier.com/locate/aescte

# Simulation of infrared detection range at fog conditions for Enhanced Vision Systems in civil aviation

# Modellrechnung der Detektionsreichweite im Infraroten bei Nebelbedingungen für erweiterte Sichtsysteme in der zivilen Luftfahrt

Kurt Beier *, Hans Gemperlein

*DLR – Remote Sensing Technology Institute, Oberpfaffenhofen, 82234 Wessling, Germany*

Received 4 June 2002; received in revised form 10 September 2003; accepted 15 September 2003

**Abstract**

The DLR project ADVISE (ADvanced VIsual System for Situation Awareness Enhancement) deals with development, simulations and testing for an Enhanced Vision System (EVS) for visual pilot assistance. Within the frame of the project ADVISE, model calculations in the infrared spectral region have been performed to investigate the influence of low visibility conditions, especially fog, for air traffic during landing approaches. The objectives of this paper are to find out whether the use of IR cameras for an EVS can improve the visibility at defined conditions of ICAO standard visual range categories CAT I, II, IIIa and IIIc for landing approaches. The calculations are carried out with the atmospheric radiative transfer model MODTRAN Version 4.0. The IR detection range is calculated in the atmospheric windows 3–5 μm and 8–12 μm and compared to the visual range defined at 0.55 μm. The sensor properties are simulated with the model TTIM (TACOM Thermal Image Model) for a specific IR camera type Thermovision 570 operating in the spectral band 8–12 μm. The influence of various climatic and seasonal meteorological conditions, aerosol types and target parameters, such as temperature and size, on the IR detection range is taken into account.


**Zusammenfassung**

Mit Modellrechnungen wird untersucht ob der Einsatz von Infrarot-Kameras zu einer Verbesserung der Sichtweite des Luftverkehrs für die Landung bei reduzierter Sicht, insbesondere bei Nebel, beitragen kann und wo die durch Atmosphäre und Sensor gegebenen Grenzen liegen. Der Einfluß der Atmosphäre auf die Detektionsreichweite im Infraroten (IR) wird mit dem Strahlungsmodell MODTRAN Version 4.0 berechnet. Die Sensoreigenschaften werden mit dem Sensormodell TTIM (TACOM Thermal Image Model) für eine IR-Kamera des Typs Thermovision 570 mit einem ungekühlten Mikrobolometer FPA (Focal Plane Array) Detektor simuliert. Es werden die Detektionsreichweiten in den atmosphärischen Fenstern 3–5 μm und 8–12 μm im IR für die Standardsichtweiten-Kategorien der Luftfahrt KAT I, II und IIIa und IIIc des Landeanflugs berechnet und mit den visuellen Sichtweiten definiert bei 0.55 μm verglichen. Der Einfluß unterschiedlicher klimatischer Verhältnisse, Aerosoltypen und Jahreszeiten sowie von Objektparametern, wie Temperatur und Größe, auf die Detektionsreichweite im IR wird berücksichtigt.


*Keywords:* Radiative transfer simulation; Infrared; Enhanced Vision System; Low visibility; Sensor model

*Schlüsselwörter:* Atmosphärisches Modell; Reduzierte Sichtbedingungen; Nebel; Luftverkehr; Landeanflug; Infrarot; Detektionsreichweite; Infrarot-Kamera

## 1. Introduction

Today's aircraft crews have to handle more and more complex situations. Critical tasks are taxiing, take-off, approach and landing especially under adverse weather con-

* Corresponding author.
*E-mail address:* kurt.beier@dlr.de (K. Beier).

1270-9638/$ – see front matter 
doi:10.1016/j.ast.2003.09.002

Fig. 1. Simulated visible scene of landing approach.

Fig. 2. Simulated IR scene of landing approach.

ditions when the runway and obstacles cannot be seen. The most promising way to increase the performance and safety of aircraft's crews is to provide comprehensive situational awareness. Besides many new approaches to enhance the situational awareness by modern flight and mission management systems or to reduce the crews's workload by flight assistance systems, a lot of research work deals with the augmentation of the visual channel [8,12]. The usage of visual information is often referred to EVS Enhanced Vision Systems. Under EVS we understand a combination of Sensor Vision and Synthetic Vision. The central feature of EVS is the data fusion of different visual information from different sources. EVS technology combines images of Infrared (IR) cameras and millimeterwave radar systems with terrain model data, precision navigation and flight attitude data. This type of image data needs a special real-time data processing to extract the information of the runway parameters and possible obstacles. The fused information is displayed in a form that can be interpreted easily by the pilot.

At daytime with optical clear atmosphere the meteorological visibility (also called "visual range") of the airspace and runway renders no troubles. Besides the natural illumination the visibility for air traffic is mainly determined by the opacity of the atmosphere. Especially at fog conditions a dramatic degradation of visibility conditions can occur culminating to a nearly undifferentiated outside world.

An upgrade of the visibility conditions can be achieved by operating sensors in spectral regions where atmospheric opacity is neglectable such as the mm-wavelength using imaging Radar [13,14] or at least lower than in the visible as in the infrared wavelength range 8–12 μm using imaging IR sensors.

The works in the DLR project ADVISE (ADvanced VIsual System for Situation Awareness Enhancement) are carried out in a two-fold way. Besides the development and testing of airworthy EVS components a simulation environment was created [3,5]. The IR simulator uses the software Vega Sensor Vision from Multigen Paradigm to generate real-time synthetic images with video frequency from the same perspective as the IR and video cameras installed in the aircraft nose. A typical simulated scene in the visible and the thermal IR given in Figs. 1 or 2, respectively, shows qualitatively the view during a landing approach under good meteorological visibility conditions. A part of this simulation works deals with the quantitative assessment of IR detection range using the atmospheric radiation code MODTRAN. The objective of this work is autonomous target recognition using an imaging IR-sensor with automated software algorithm to detect and identify the runway and obstacles. Human perception, which means man in the loop of the IR-sensor with display, is not regarded here.

The objectives of this paper are to find out whether the use of IR cameras with autonomous target recognition (ATR) can improve the range to detect objects compared to the human visual ranges at defined meteorological conditions – especially at fog – of ICAO (Internatinal Civil Aviation Organisation) standard visual range categories CAT I, II, IIIa and IIIc for landing approaches. We operate an imaging IR-sensor with automated software algorithm to detect and identify the runway and relevant obstacles. With simulation calculations we compare the achievable IR detection range for a typical state of the art IR camera at defined conditions of ICAO standard visual range categories CAT I, II, IIIa and IIIc for landing approaches with the visibility in the visual range. Simulations are performed in two steps. First we determine the transmission of the atmosphere and the limitation due to atmosphere alone, corresponding to the use of an ideal sensor. In the second step we include the additional influence of the sensor properties and target parameters and determine the detection range. Simulations are performed for different climates and seasons, such as winter and summer in subarctic, temperate zones and tropics. Also different types of prevailing local atmospheric aerosols, such as rural, urban, maritime or desert, are taken

into account to show possible variations of IR-visibility at airports all over the world.

In Section 2 we describe the meteorology and physical basics of visibility degradation in a foggy atmosphere. The used ICAO classification for runway visibility and decision heights for landing approaches are given.

In Section 3 the used atmospheric radiation transfer model MODTRAN, the sensor model TTIM (TACOM Thermal Image Model) and the target model are introduced. The used climate and aerosol models for the atmosphere are given.

The definition and the method to determine the detection range for the autonomous IR camera are described in Section 4.

The used input data for the atmospheric and sensor models and associated assumptions are summarized in Section 5.

In Section 6 we present the results of the model calculations. First we show the spectral transmission for different meteorological conditions in the two IR bands 3–5 μm and 8–12 μm compared to the visual range at 0.55 μm. Then the IR detection ranges of the IR camera are given at defined landing categories for varying target size and temperature. The results include the optimal detection range for an ideal IR sensor, which is equivalent to the atmospheric limitation, and the realistic achievable detection range for a real IR sensor with limited spatial and radiometric resolution.

In Section 7 we summarize the results and discuss possible improvements of the detection range for the different visual range categories by application of IR imaging sensors and their limitations.

## 2. Radiative properties of fog

If air is almost saturated with water vapor (relative humidity close to 100%), fog can form in the presence of a sufficient number of condensation nuclei. The saturation of air can be the result of two different processes; one is the mixing of two air masses with different temperature and/or humidity generating advection fog, the other process is radiative cooling of the air close to the dew point resulting in radiative fog. The foggy atmosphere is a turbulent mixture of gas and particles.

Fog impairs propagation of electromagnetic radiation in the atmosphere for all wavelength $<1$ cm ($>30$ GHz) by scattering and absorption at fog particles. In fog conditions scattering is the dominant process of radiative transfer. The amount of absorption and scattering depends on the microphysical structure of fog particles (aerosols).

The essential microphysical parameters of aerosols are: chemical composition of condensation nuclei, size distribution and liquid water content. Generally tropospherical aerosols show a great manifold in chemical composition, geometry, and size distribution. Typical aerosols have radii of $10^{-4}$–1 μm, but can grow up to diameter of 30 μm in fog. The small particles with radii between 0.1–1.0 μm scatter strongest in the visible region, whereas the larger particles scatter stronger in the IR region [15,17,18].

The scattering cross sections of aerosols can be characterised for the special case of a sphere with homogeneous refractive index, by the classical Mie scattering theory. The scattering cross section of a particle with radius $r$ depends strongly on the nondimensional ratio $2\pi r/\lambda$, where $\lambda$ is the wavelength of radiation. The maximum of the scattering cross section occurs, when the particle radius is equal to the wavelength of radiation. The actual particle distribution in the atmosphere shows a number of varying sizes described with its size distribution. Therefore an effective scattering cross section of each size distribution has to be found. In fog conditions particles absorb water and grow considerably in their size. The effect in the visible is that scattering becomes less dependent of wavelength, which means more 'white'; in the IR region however scattering gets stronger. The question whether scattering in the IR is less than in the visible range therefore depends to what size the particles are swelling. An average size less than 1 μm yields a considerable smaller scattering cross section in the IR. If the particles swell to an average size of 5 to 10 μm then circumstances arise where there is no significant difference in scattering between the IR and visible spectral band: The visibility is equally bad [2,9,11,16].

The reason for degradation of visibility in foggy atmosphere is first of all scattering of natural or artificial illumination at aerosols. The observed radiation consists of two contributions, the radiation of the target attenuated by atmosphere and the scattered (and emitted IR) radiation along the atmospheric path between target and observer. The second process reduces the contrast of target to surrounding background and causes a real loss of information.

For aviation the visibility conditions for landing approach are classified in three ICAO standard categories, named CAT I, CAT II and CAT III. This classification facilitate the pilot the decision to continue or terminate the landing approach at a predetermined flight altitude. Table 1 summarises the definition of CAT conditions of runway visual range and decision heights for landing. The runway visual range is equal to the meteorological visibility for a horizontal path at ground level as used in the atmospheric model MODTRAN. The assumptions for a typical landing approach are an angle for glide path of 3° and a flight velocity of 200 ft/s (61 m/s).

Table 1
ICAO categories of runway visual range and decision height for landing

| Category CAT | Decision height ft (m) | Visual range ft (m) |
|---|---|---|
| I | 200 (61) | 4000 (1220) |
| II | 100 (30) | 2000 (610) |
| IIIa | 50 (15) | 1000 (305) |
| IIIc | 50 (15) | 300 (92) |

Table 2
MODTRAN climate and aerosol models: climate models for troposphere 0–10 km with profiles: spring/summer and autumn/winter aerosol models for planetary boundary layer 0–2 km

| Climate | Aerosol |
|---|---|
| Tropical | Rural |
| Midlatitude summer | Maritime |
| Midlatitude winter | Rural |
| Subarctic summer | Advection fog |
| Subarctic winter | Radiative fog |
| US Standard | Desert |
| User defined | User defined |

## 3. Radiation and sensor model

### *3.1. Atmospheric radiation model*

For the calculation of the atmospheric radiation transfer we use the radiation model MODTRAN (Moderate Resolution Propagation Model) Version 4.0 [1]. The model enables the calculation of transmission and radiance of any atmospheric path in a wide spectral range from UV at 0.2 μm, the visible and IR region up to the millimeterwave region with a spectral resolution of 1 $cm^{-1}$. MODTRAN offers six climate models for different geographic latitudes and seasons, shown in Table 2, which define pressure, temperature and mixing ratio of 25 atmospheric species for more than 50 atmospheric layers from sea level to 120 km altitude. The aerosol models for the planetary boundary layer close to surface are strongly influenced by local properties of earth surface and weather, so that we distinguish rural, maritime, urban and desert environment as well as fog and rain. A number of cloud models can be selected for different altitudes, appearance, and thickness of layers in combination with different rain rates and vertical rain profiles. Furthermore it is possible to include user defined atmospheric and aerosol data from own meteorological measurements.

### *3.2. Sensor model*

Radiative transfer through the atmosphere is only one effect that influences the detection range of IR systems. The limited spatial resolution of the optics and the detector, and the noise of detector and signal processing reduces also the contrast radiance of target to background. The influence of the IR sensor's transfer functions on the contrast radiance is simulated with the model TTIM [7] which is a part of the model PRISM (Physically Reasonable IR-Signature Model) [6].

For this we need a radiance image of a target with background. This is realized with a quadratic bar resolution pattern consisting of 7 homogeneous vertical bars (see Fig. 7). Four bars have the surface temperature of the target and the intermediary bars show background temperature. As we assume an IR camera with ATR, without taking into account human perception, the choice of the target pattern is uncritical. The model TTIM enables to simulate different types of IR sensors such as a scanning and staring system with focal plane arrays (FPA). All essential noise sources of the system (background photon noise, trapped state noise, reset noise, dark current noise, charge transfer noise, output amplifier noise and fixed pattern noise) are modeled. The influence of the sensor is calculated with the MTF (Modulation Transfer Function) in the frequency domain. The NETD (Noise Equivalent Temperature Difference) is used to characterise the combined noise of detector and signal processing.

## 4. Method to determine IR detection range

The contrast radiance $\Delta L(r) = L_T - L_B$ as radiance difference of target and background is calculated in the visible (VIS) 0.4–0.8 μm as a function of range on the slant path from aircraft to ground. The contrast $C$ of target and background is defined as ratio of the contrast radiance $L$ and the background radiance $C(r) = \Delta L/L_B$. By means of normalising of the contrast $C$ to the initial contrast $C(0)$ at range $r = 0$ we achieve the contrast transmission $\tau_C(r) = C(r)/C(0)$. The contrast transmission as a function of range is used in the visible band to describe the efficiency of atmospheric transfer. In the visible band the meteorological visibility is defined as the range where initial contrast transmission $\tau_C(0) = 1.0$ is decreased to $\tau_C(r) = 0.02$ or 2% [4]. In the visible band the initial contrast $C(0)$ of a black nonreflective target observed against the horizon is always identical to one.

For evaluation of the IR detection range caused by the atmosphere and the sensor we use the equivalent temperature difference $\Delta T(r) = T_T - T_B$, applied to the bar resolution pattern. The detection range of the IR camera including atmosphere plus sensor is defined as the range where the NETD is equal the radiation temperature difference $\Delta T(r) = \text{NETD}$.

## 5. Input data for models

The input data for the MODTRAN atmospheric model are specific climates and aerosols, the visibility according the ICAO categories, the geometry and length of the atmospheric path, and the temperature and emissivity of target and background. For the calculations with visibility category I, which is 1220 m runway visual range, we chose all climate models listed in Table 2. Each of this climate models is combined with the aerosol models rural, maritime and urban. For the visibility category II and III we use fog models, the radiative fog or advection fog respectively, in combination with the climate model midlatitude winter. For the fog models differences concerning the origin of the condensation nuclei become insignificant, because liquid water is the predominant constituent of the fog aerosol.

Table 3
Ground temperature for climate models

| Climate | Temperature [K] |
|---|---|
| Tropical | 299.7 |
| Midlatitude summer | 294.2 |
| Midlatitude winter | 272.2 |
| Subarctic summer | 287.2 |
| Subarctic winter | 257.2 |

Table 4
Technical data of IR camera

| Detector type | Microbolometer, uncooled |
|---|---|
| Detector material | Vanadium oxide on silicon |
| Detector array | 320 × 240 elements FPA |
| Spectral range | 7.5–13 µm |
| Spatial resolution | 0.65 mrad – $f = 72$ mm lens |
| | 1.3 mrad – $f = 36$ mm lens |
| Field of view | 12° × 6° or 24° × 12° |
| Radiometric resolution | 0.15 K–300 K |
| Video rate | 50 frames/sec |
| Detector time constant | ∼14 msec |

The atmospheric calculation is carried out one-dimensional along the line of sight between observer (aircraft) and target (runway) and background which is always a slant path with zenith angle 93° (−3° elevation angle) with variable length from 50 m to 10 km. The emissivity of the runway (asphalt) and the terrain background is assumed constant $\varepsilon = 0.9$. The background temperature is assumed to be equal to the ground layer of the particular atmospheric model. The target temperature difference of $\Delta T = +1$ K, $+10$ K, $+40$ K or $+100$ K is based on this background temperature. Typical observed daily and seasonal variations of the apparent temperature difference for the runway are in the range of 2 K to 20 K.

The low temperature difference represents the runway, whereas higher differences could be attributed to a car or an aircraft on the runway. The terrain background temperature for the used climate models are given in Table 3.

The influence of the sensor parameters and target size is simulated two-dimensionally with simulated IR images. The technical data of the IR camera type Thermovision 570 are listed in Table 4. The used MTF and NETD of the IR camera are based on experimental tests carried out at FOM [10]. For simulation we defined one large and two small targets. The runway is assumed to represent the large target. The two small targets have sizes of 5 m × 5 m and 2 m × 2 m and are formed as square shaped bar patterns.

## 6. Results

### *6.1. Spectral transmission of the atmosphere*

The spectral transmission of the atmosphere for varying ranges enables a simple qualitative comparison of the visibility in different atmospheric windows. The spectral transmission for CAT I with midlatitude summer and rural aerosol for different ranges is shown in Fig. 3. In the visible spectral band the transmission is significantly lower than in both IR windows. Reducing visibility to CAT II conditions with radiative fog only the IR band 8–12 µm is superior to the visible as shown in Fig. 4. Finally at CAT IIIa conditions

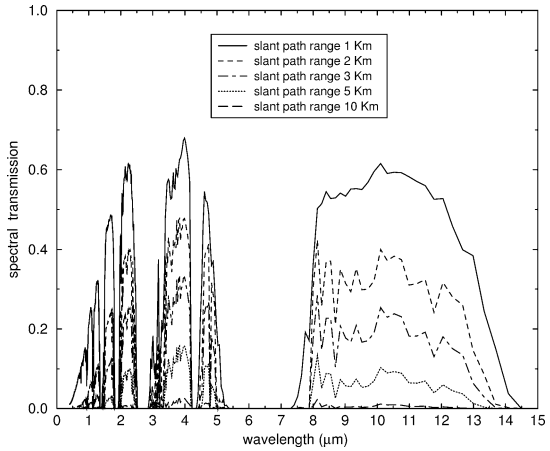


Fig. 3. Spectral transmission for CAT I conditions runway visual range 1220 m (4000 ft); atmospheric model: midlatitude summer, rural aerosol.

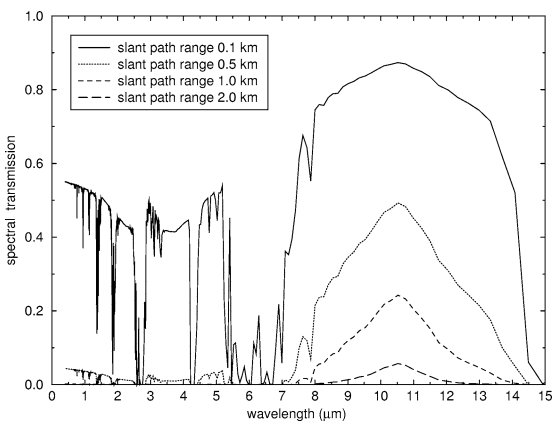


Fig. 4. Spectral transmission for CAT II conditions runway visual range 610 m (2000 ft); atmospheric model: midlatitude winter, radiative fog.

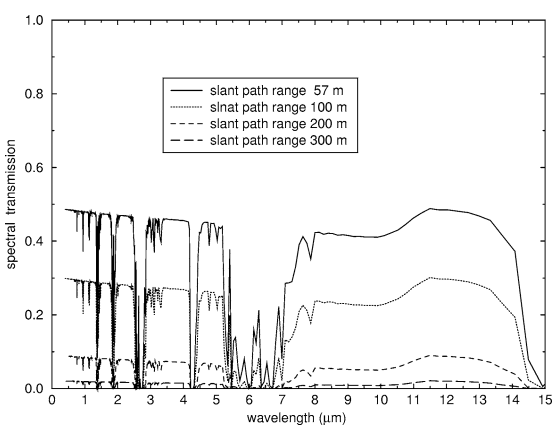


Fig. 5. Spectral transmission for CAT IIIa conditions, runway visual range 305 m (1000 ft); atmospheric model: midlatitude winter, advection fog.

with visibility of 300 m shown in Fig. 4 there are no more substantial differences for the spectral transmission in all spectral bands.

The transmissions enable to compare quantatively the quality of atmospheric radiation transfer. Any detection process of EO systems on an atmospheric path is based on the atmospheric transmission and the contrast radiance between target and the background. The transmission alone is not a figure of merit for the IR camera, but the comparison of visual and IR transmission shows whether the atmosphere favours or discriminates an IR spectral band concerning radiative transfer.

The IR detection range at CAT I conditions depends strongly on the climate and the prevailing type of aerosol. We compare the spectral transmission for 5 different climates with the same maritime aerosol. At high absolute humidity in the cases of tropical atmosphere or summer we expect lower IR detection ranges than for conditions with low humidity in winter. The best IR detection range in the spectral band 8–12 μm is achieved with midlatitude winter. An additional factor influencing the contrast radiance and therewith the IR detection range is the value of the background temperature as reference for the temperature difference of the target. In the subarctic winter the lowest humidity occurs but the background temperature 257 K is the lowest, too. The available initial contrast hence is lower than for the midlatitude winter where the background temperature amounts to 272 K.

A comparison of different aerosol models shows that the maritime aerosols always result in the lowest detection range in the IR independently of the climate model. The rural and urban aerosols produce noticeable greater detection ranges in the IR. The reason for this is the varying size distribution of the aerosols. Maritime aerosols have in average larger particle radii than rural or urban aerosols, and therefore the Mie scattering in the IR is stronger.

In the case of visibility category CAT II with radiation fog, the thermal IR region 8–12 μm shows a substantially better performance than the visual or middle IR range as depicted in Fig. 4. The reason for this is based again on the particle size distribution for radiation fog. Under moderate fog conditions the majority of aerosol particle have average radii of about 1 μm and only few fog particles have larger radii. Therefore scattering in the visual and middle IR range is strong and in the long wave thermal IR range corresponding weaker.

### *6.2. Influence of the atmosphere on the IR detection range*

In Table 5 the IR detection range in terms of NEDT threshold only caused by the atmosphere is given for all categories of runway visual range in two IR bands, assuming a temperature difference of 10 K between a large target (runway) and the background. This detection range may represent an ideal IR sensor with MTF $\equiv 1$ or unlimited spatial resolution. The detection range there is independent of the target size. For CAT I the IR detection range is given in a range span, representing the variation with different climate and aerosol models. In the TIR the lowest visibility is obtained for the tropical climate at high absolute humidity of air in combination with maritime aerosols. These conditions represent an airport in the tropics located near the coast. The best IR detection range occurs in winter with low absolute humidity of air and rural aerosol.

Table 5
Calculated detection range (km) in the IR for different CAT conditions, temperature difference of target to background $\Delta T = 10$ K, detection range defined at NEDT threshold 0.15 K

| CAT | Visibility | Detection range (km) | |
|---|---|---|---|
| | VIS | MIR | TIR |
| | 0.55 μm | 3–5 μm | 8–12 μm |
| I | 1.22 | 3.0–9.8 | 5.9–10.1 |
| II | 0.61 | 0.54 | 2.4 |
| IIIa | 0.305 | 0.294 | 0.293 |
| IIIc | 0.092 | 0.089 | 0.087 |

In the middle IR region MIR the detection range is reciprocally best at climatic conditions with high temperatures as summer or tropical atmosphere. All IR detection ranges for CAT I conditions are noticeable superior to the visual ranges for all climates and types of aerosols. For CAT II conditions we achieve a noticeable improvement for the IR detection range by a factor 4 only in the thermal IR band TIR 8–12 μm. The middle IR band MIR yields no improvement for the detection range.

For strong fog in the cases CAT IIIa and CAT IIIc the visibility or detection range respectively, is similar low in all spectral bands. The atmosphere is the limiting factor. Like in the visual range, the detection range in the IR also depends on the initial contrast radiance of target to background. In the thermal IR the difference of temperature and emissivity determines the initial contrast radiance. Assuming the same emissivity of $\varepsilon = 0.9$ for target and background, the target temperature was varied. Fig. 6 shows for an IR camera with an ideal MTF $\equiv 1.0$, the influence of an increasing initial target-background temperature difference on the observable radiation temperature difference vs. slant path range and the resulting IR detection range. The IR detection range including the IR sensor is defined as the range where the radiation temperature difference is equal the system NETD. The NETD of the IR camera is assumed to be 0.15 K.

If the temperature difference $\Delta T$ is raised from 1 K to 10 K the IR detection range increases from 1.1 km to 2.4 km. At a temperature difference of 40 K we achieve 3.3 km and if the temperature difference amounts to 100 K the IR detection range is 4.0 km. It seems to be realistical that large temperature differencies on large areas are unlikely to observe for natural surfaces or a runway. However artificial targets like vehicles or aircraft may exhibit small hot areas or spots of their engine and exhaust facilities acting as hot point radiation source.

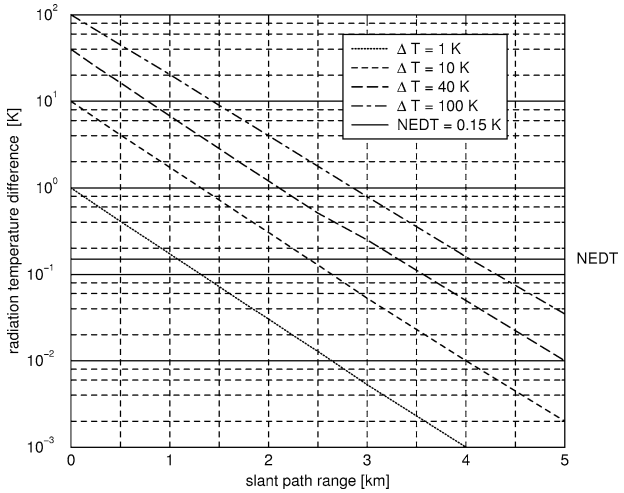


Fig. 6. Radiation temperature difference of target to background vs. slant path range ideal sensor with MTF ≡ 1.0; TIR 8–12 µm, CAT II visual range 2000 ft (610 m); parameter: initial temperature difference of target to background $\Delta T = 1$ K, 10 K, 40 K, 100 K; NETD Noise Equivalent Temperature Difference of IR camera, here: 0.15 K.

### 6.3. *Influence of the sensor on IR detection range*

After the simulation of the atmospheric influence on the IR detection range the sensor transfer characteristics is taken into account in the next step. The limited spatial and radiometric resolution of the IR camera, caused by the optics, the IR detector and the system noise, results in an additional reduction of the detection range referred to a defined target. The apparent angular size of the target determines the achievable IR detection range.

The simulation of the sensor transfer properties is carried out with the model TTIM using the defined bar resolution pattern at different ranges.

The result of the sensor simulation is represented in Fig. 7 as a sequence of images of the resolution pattern in stages beginning with the initial situation at the target up to the image at the sensor display. The resulting radiation temperature difference $\Delta T(r)$ in the resolution pattern is evalutated along a (video) line across the bar pattern.

The initial situation in Fig. 7(a) shows four resolution patterns at different ranges without atmosphere and sensor. The radiation temperature difference of the bars amounts independently of the apparent target size always to 10 K. The background temperature of the bright bars is 272.2 K. The size of the pattern, beginning top left counterclockwise, is equivalent to the spatial frequencies 0.25, 0.33, 0.5 and 1.0 cycles/mrad. This is converted to ranges 0.5, 0.667, 1.0 and 2.0 km for a target size 2 m × 2 m.

Fig. 7(b) demonstrates the influence of the atmosphere with increasing range for the case CAT II with visibility 610 m for radiative fog. The four resolution patterns show different radiation temperature differences, whereas the quality of the images remains unmodified. The radiation temperature difference of 10 K now decreases proportionally

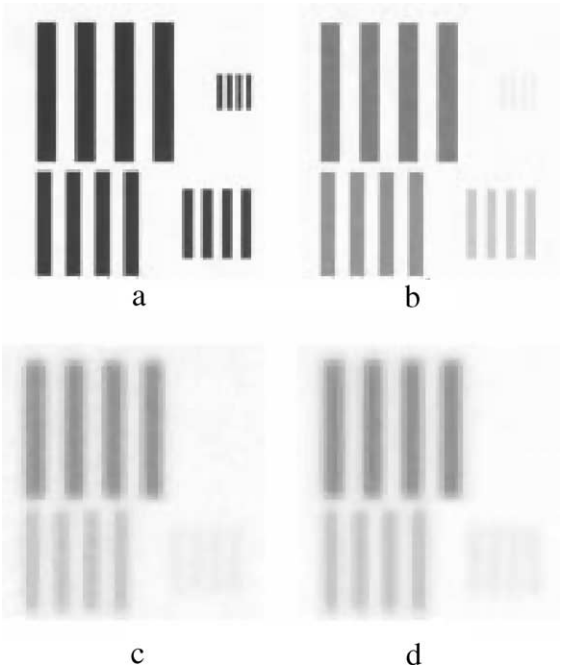


Fig. 7. Contrast reduction for resolution pattern as a function of range for TIR 8–12 µm: (a) initial situation: $\Delta T = 10$ K, $T_B = 272.2$ K, $\varepsilon = 0.9$ left top counterclockwise: range = 0.5 km, 0.667 km, 1.0 km, 2.0 km; resolution pattern: target size 2 m × 2 m; spatial resolution: 0.25 cycles mrad$^{-1}$, 0.33 cycles mrad$^{-1}$, 0.50 cycles mrad$^{-1}$, 1.00 cycles mrad$^{-1}$; (b) atmosphere only: CAT II visual range 610 m, midlatitude winter, radiative fog resulting radiation temperature differences: 4.10 K, 3.26 K, 1.72 K, 0.31 K; (c) atmosphere and sensor MTF: IFoV = 0.65 mrad resulting radiation temperature differences: 3.41 K, 2.10 K, 0.58 K, 0.01 K; (d) atmosphere, sensor MTF and noise: NETD = 0.15 K.

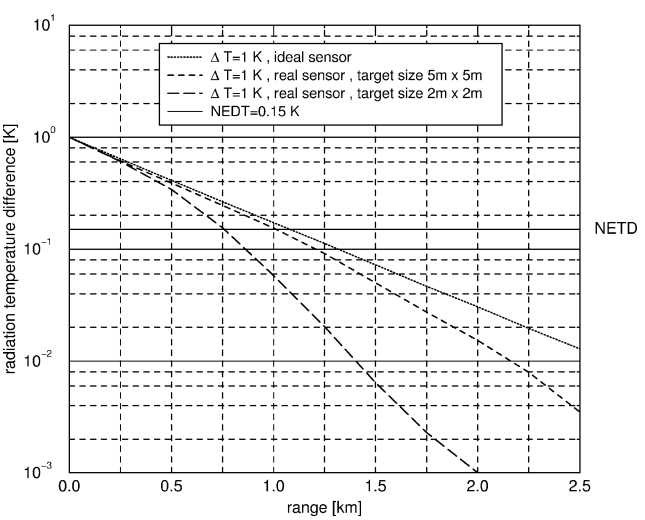


Fig. 8. Comparison of radiation temperature difference for real and ideal IR sensor vs. slant path range TIR 8–12 µm, CAT II visual range 2000 ft (610 m), MTF and noise of IR camera type Thermovision 570 temperature difference target-background $\Delta T = 1$ K parameter: target size.

with the range to 4.1 K at 0.5 km, 3.26 K at 0.667 km, 1.72 K at 1.0 km and 0.31 K at 2.0 km.

Fig. 7(c) depicts clearly the influence of the sensor imaging properties. The bar resolution becomes blurred at

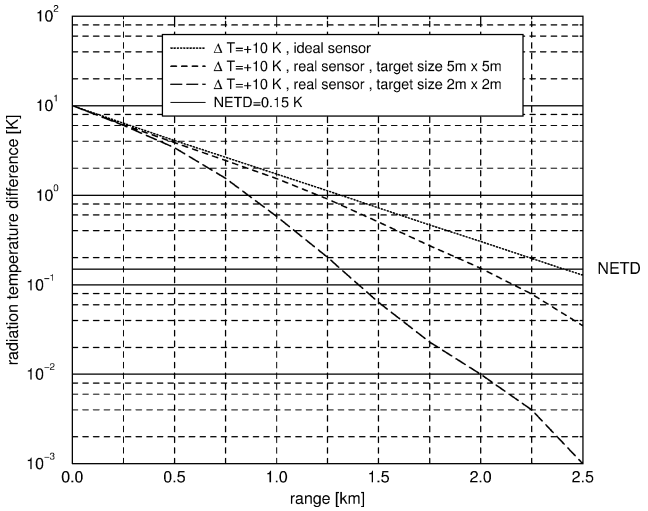


Fig. 9. Comparison of radiation temperature difference for real and ideal IR sensor vs. slant path range TIR 8–12 µm, CAT II visual range 2000 ft (610 m), MTF and noise of IR camera type Thermovision 570 temperature difference target-background $\Delta T = 10$ K parameter: target size.

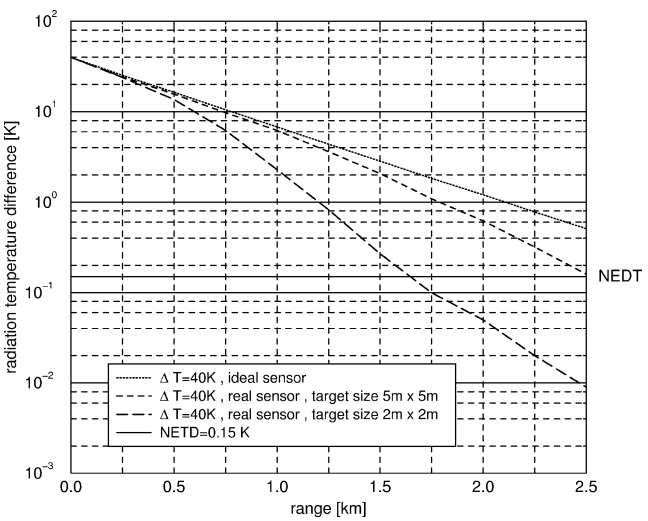


Fig. 10. Comparison of radiation temperature difference for real and ideal IR sensor vs. slant path range TIR 8–12 µm, CAT II visual range 2000 ft (610 m), MTF and noise of IR camera type Thermovision 570 temperature difference target-background $\Delta T = 40$ K parameter: target size.

the edges, especially the contrast for the small pattern is mostly decreased. The radiation temperature difference of the pattern decreases further with increasing range, 3.41 K at 0.5 km, 2.1 K at 0.667 km, 0.58 K at 1.0 km and 0.01 K at 2.0 km.

Fig. 7(d) at last shows the influence of the statistical system noise with a noise equivalent temperature difference of NETD = 0.15 K. The quality of the images is only marginally impaired. The essential losses of contrast are due to the atmosphere and the sensor MTF.

Fig. 8 shows the radiation temperature difference as a function of range at CAT II conditions for varying target size with the initial temperature difference $\Delta T = 1$ K. The top curve represents the ideal sensor or a large target as the runway. The curve for a real sensor with limited spatial resolution and target size of 5 m × 5 m is still close to the ideal sensor curve. For the small target of 2 m × 2 m however there is already a strong decay reducing the attainable visibility noticeably. The radiation temperature vs. range for the higher initial temperature difference $\Delta T = 10$ K or $\Delta T = 40$ K is shown in Figs. 9 or 10 respectively. The resulting IR detection ranges for the threshold NETD = 0.15 K are summarized in Table 6. For CAT II conditions the use of IR cameras in the 8–12 µm spectral can improve the IR detection range compared to the meteoroligical visibility substantially. The IR detection range of the IR camera is persistently higher than 0.75 km for all targets. For large targets as the runway the category CAT II is improved to CAT I.

Table 6
IR detection range (km) of ideal and real IR sensor with varying target sizes and temperature differences CAT II visual range 2000 ft (610 m), radiative fog, spectral band 8–12 µm, threshold NETD = 0.15 K

| IR sensor/target size | Temperature difference $\Delta T$ (K) | | | |
|---|---|---|---|---|
| | 1 | 10 | 40 | 100 |
| ideal/any | 1.1 | 2.4 | 3.3 | 4.0 |
| real/5 m × 5 m | 1.0 | 2.1 | 2.5 | 3.2 |
| real/2 m × 2 m | 0.75 | 1.2 | 1.6 | 2.1 |

## 7. Summary and conclusions

Model calculations have been performed in the thermal infrared regions 3–5 µm and 8–12 µm to assess the use of IR cameras in low visibility conditions, especially fog, for air traffic during landing approaches. The investigations are carried out with the atmospheric radiative transfer model MODTRAN version 4.0 and the thermal imaging model TTIM. The ICAO standard visual range categories CAT I, II, IIIa and IIIc are used as bench marks. The influence on visibility of various climatic and seasonal meteorological conditions, aerosol types and target parameters, such as temperature and size, is taken into account. The simulation uses sensor parameters of a standard uncooled IR camera type Thermovision 570, which is utilized for flight measurement at DLR within the Enhanced Vision Project ADVISE. The instantaneous field of views are 0.65 mrad or 1.3 mrad respectively.

The results can be summarized as follows: At CAT I conditions with a visual range 1220 m both IR spectral bands can achieve IR detection ranges, in terms of the defined NEDT = 0.15 K, from 3 to 10 km. The IR detection range is noticeable improved for all climatic zones, seasons and types of aerosols. The lowest IR detection range is met in the tropics at sea level with high absolute humidity. In the thermal IR 8–12 µm the most favourable terms occur at subarctic winter with low humidity. The IR detection range referring to small targets with a size of 2–5 m is limited due to the sensor MTF. For large targets such as the runway

the atmospheric influence is the limiting factor for the IR detection range.

For CAT II conditions at moderate fog, with 610 m visual range, only the thermal IR region 8–12 μm enables to improve of the detection range up to 1–2 km, which means CAT II conditions can be improved to CAT I. The selected spatial and radiometric resolution of the IR sensor has to fit to the size and temperature difference of the target to be detected. The supposed IR sensor requires for a target with dimensions 5 m × 5 m a minimum temperature difference of 1 K to the ambient background.

For categories CAT IIIa and IIIc with dense fog and visual ranges of 300 m to 100 m and less, there is no improvement achievable utilizing IR cameras. The atmosphere is the limiting factor in all spectral bands from the visible to the IR. Even a large initial radiation temperature difference of 100 K and more cannot improve the IR detection range significantly. At this atmospheric conditions an IR sensor even with a smaller NEDT, which means higher radiometric resolution, would only enhance the inhomogeneities of the atmospheric path radiance and not improve the IR detection range of the target. In this case an imaging radar system is necessary in order to improve the visibility for landing approaches. However for a taxiing aircraft on ground it makes sense to use IR cameras even at dense fog conditions to improve detection and recognition of obstacles such as persons, vehicles and ground installations within the range of the IR detection range.

The validation of the simulation results with flight measurements is still in progress. A comparison of measured and simulated data will be presented in a succeeding paper and a final report.

## Acknowledgements

We would like to thank our colleague P. Haschberger for many helpful discussions and comments.

## References

[1] G.P. Anderson, A. Berk, L.S. Bernstein, M.W. Matthew, S.M. Adler-Golden, B.C. Robertson, P. Acharya, J.H. Chetwynd, F.X. Kneyzis, E.P. Shettle, L.W. Abreu, W.O. Gallery, J.E.A. Selby, S.A. Clough, MODTRAN User's Manual Versions 3.7 and 4.0, Technical Report, Air Force Research Laboratory, Hanscom AFB, MA 01731-3010, USA, 1998.

[2] K. Beier, R. Böhl, W. Hahn, V. Tank, G. Wagner, H. Weisser, Measurement and modelling of infrared imaging systems at conditions of reduced visibility (fog) for traffic applications, in: Conference Proceedings, vol. 2223, SPIE, 1994, pp. 175–186.

[3] K. Beier, J. Fries, R. Mueller, G. Palubinskas, In measurements and image processing for enhanced vision systems in civil aviation, in: J.G. Verly (Ed.), in: SPIE Aerosense Conference, Enhanced and Synthetic Vision 2001, vol. 4363, 2001, pp. 207–218.

[4] H. Blackwell, Contrast thresholds of the human eye, J. Opt. Soc. Am. 36 (1946) 624–643.

[5] H.U. Doehler, D. Bollmeyer, Simulation of imaging radar for obstacle avoidance and enhanced vision, in: J.G. Verly (Ed.), SPIE Aerosense Conference, Enhanced and Synthetic Vision 1997, vol. 3088, 1997, pp. 64–72.

[6] T. Gonda, G.R. Gerhardt, A comprehensive methodology for thermal signature simulation of targets and backgrounds, in: Conference Proceedings: Aerospace Pattern Recognition, vol. 1098, SPIE, 1989, pp. 23–27.

[7] C.S. Hall, E.T. Buxton, T.J. Rogne, TACOM Thermal Image Model, Version 3.1, Technical Reference and User's Guide, Technical Report, Optimetrics Inc. Michigan USA, Report Nr. OMI-405, 1989.

[8] P. Hecker, Aircrew assistance by sophisticated vision systems, in: International Workshop on Technical Elements for Aviation Safety, Tokyo, Japan, 1999, pp. 1–34.

[9] D.H. Höhn, W. Steffen, A. Kohnle, Atmospheric IR Propagation, Technical Report 1984/17, Forschungsinstitut für Optik FfO Tübingen, 1984.

[10] A. Kohnle, Experimentelle Untersuchungen der Leistungsdaten des handgehaltenen WBG's Thermovision 570 von der Firma AGEMA, Technical Report, Forschungsinstitut für Optik, FfO Nr. 1997/122, 1997.

[11] N.S. Kopeika, Effects of aerosols on imaging through the atmosphere: A review of spatial frequency and wavelength dependent effects, Optical Engineering 24 (4) (1985).

[12] B. Korn, H.U. Doehler, P. Hecker, Millimeterwave radar data processing for enhanced vision systems, in: J.G. Verly (Ed.), SPIE Aerosense Conference, Enhanced and Synthetic Vision 1999, vol. 3691, 1999, pp. 29–38.

[13] B. Korn, H.U. Doehler, P. Hecker, Robust sensor data fusion for board autonomous navigation during approach and landing, in: Intl. Symposium on Precision Approach and Automatic Landing, ISPA2000, Munich, 2000, pp. 451–457.

[14] B. Korn, H.U. Doehler, P. Hecker, Weather independent flight guidance: Analysis of mmw radar images for approach and landing, in: 15th International Conference of Pattern Recognition, ICPR2000, Barcelona, vol. I, 2000, pp. 350–353.

[15] J.D. Lindberg, Early wintertime Fog and Haze (Report on Project Meppen 80), Technical Report ASL-TR-82-0180, US Army Atmospheric Science Laboratory, White Sands Missile Range, NM, 1982.

[16] R. Neuwirth, Extinction properties of visible-, IR- and mm-radiation (94 GHz), in: Third International Conference on Advanced Infrared Detectors and Systems, London, 1986.

[17] E.P. Shettle, Models of aerosols, clouds and precipitation for atmospheric propagation studies, in: AGARD Conference Proceedings No. 454, Atmospheric Propagation in the UV, Visible, IR and MM-Wave Region and Related System Aspects, AGARD, 1990.

[18] E.P. Shettle, R.W. Fenn, Models of the aerosols of the lower atmosphere and the effects of humidity variations on their optical properties, Scientific Report AFGL-TR-79-0214, Air Force Geophysics Laboratory, Hanscom AFB, MA, 1979.